A digital nonlinear piezoelectric tuned vibration absorber

G Raze[1], A Jadoul[2], S Guichaux[2], V Broun[2] and G Kerschen[1]

[1] Space Structures and Systems Laboratory, Aerospace and Mechanical Engineering Department, University of Liège, Quartier Polytech 1 (B52/3), Allée de la Découverte 9, B-4000 Liège, Belgium

[2] Service d'Electronique, Département Ingénieur Industriel, Haute Ecole de la Province de Liège, Quai Gloesener 6, B-4020 Liège, Belgium

E-mail: g.raze@uliege.be

Abstract. This study presents the practical realization of a digital vibration absorber that, owing to the flexibility provided by the digital unit, synthesizes linear and nonlinear shunt circuits. The absorber, composed of a microprocessor and a current source, is connected to the host structure with piezoelectric patches. The performance of both circuits is compared experimentally for a nonlinear host structure. The superiority of a properly-tuned nonlinear absorber over its linear counterpart is validated, but the limits of the nonlinear absorber are also explored. Moreover, the accuracy of the tuning procedure and formulas is assessed through experimental parametric studies.

Keywords: piezoelectric vibration absorber, synthetic impedance, nonlinear vibrations, nonlinear vibration absorber, principle of similarity

1. Introduction

Since the seminal works of Forward [1] and Hagood and von Flotow [2], piezoelectric shunt damping has become a widespread technique to reduce unwanted vibrations in structural systems. This approach relies on the transducing capability of a piezoelectric material, i.e., its ability to convert part of its mechanical energy into electrical energy. This electrical energy may then be dissipated by connecting properly tuned shunt circuits to the transducer. A popular shunt circuit is the resonant series RL one, in which the inductance and resistance are tuned so that the maximum vibratory amplitude of the controlled structure under harmonic loading is minimal. The exact inductance and resistance values leading to this H_∞-optimal solution were derived by Soltani et al [3]. This strategy results in the so-called *equal-peak design*, because the frequency response function of the controlled structure exhibit two resonance peaks of equal amplitude. A recent paper by Ikegame et al [4] gathers tuning formulas for usual configurations and objectives at hand. Gripp and Rade [5] reviewed a number of works and applications of piezoelectric shunt damping. Interestingly, absorbers relying on the resonance of an added device also come in various forms and are used in a variety of domains. Examples include tuned mass dampers [6], Helmholtz resonators in acoustics [7] and plasmonic absorbers for opto-electronic devices [8, 9, 10]. Resonance can be a desirable feature in some applications, for instance high-performance infrared sensors [11].

Piezoelectric tuned vibration absorbers (PTVA) rely on a precise *tuning* of the electrical resonance frequency according to that of the host structure. The latter may be variable due to, e.g., time-varying characteristics or structural nonlinearities. Hence, this technique is often considered as lacking robustness. This is why Agnes and Inman [12] investigated the effect of adding nonlinear elements in the shunt circuit. They found that the bandwidth of the piezoelectric absorber could be increased; however, undesirable nonlinear phenomena such as quasiperiodic and chaotic motions could also be observed. Along the same lines, Richard et al utilized continuous switching of a piezoelectric shunt to realize a nonlinear absorber [13]. In [14], Zhou et al explored a piezoelectric nonlinear energy sink (NES) comprising an essential nonlinearity made of a ferroelectric capacitor and a negative capacitance circuit. Because this absorber has no preferential resonance frequency, it can pump the energy from the host structure in an irreversible fashion. This energy transfer is, however, conditioned upon an energy threshold, i.e., the transfer does not occur if the vibrational energy of the host structure is not large enough. Based on a *nonlinear principle of similarity*, Soltani and Kerschen [15] introduced a nonlinear PTVA. The absorber nonlinearity is similar to that present in the host structure, so that the host structure and absorber frequencies evolve in a similar way when the forcing amplitude changes, which, in turn, increases the range of forcing amplitudes over which the nonlinear PTVA is effective.

Focusing now on experimental demonstrations, a nonlinear absorber relying on the saturation phenomenon was realized through digital control in [16] and [17]. The first practical implementation of a nonlinear PTVA was achieved in [18] whereas Silva et

al [19] realized a piezoelectric NES using analog electronics. An interesting feature of [18] is that the use of synthetic inductors (and, thus, of a power supply) was avoided, leading to a fully passive piezoelectric absorber. We also note that different nonlinear absorbers, including an NES and an NLTVA were realized experimentally using a tunable magnetic vibration absorber [20].

The objective of the present study is to realize PTVAs to mitigate structural vibrations through synthetic impedances, following the idea proposed by Fleming et al [21]. The innovation of this work is that the full flexibility of the digital absorber is exploited to implement arbitrarily complex nonlinear laws, something which is not easily achievable using purely mechanical elements, hence, paving the way for a more widespread use of nonlinear absorbers in real-world applications.

The paper is organized as follows. Section 2 briefly reviews the theory behind the tuning of linear and nonlinear PTVAs. Section 3 introduces the proposed digital absorber and discusses its various components. In Section 4, experimental tests of a digital linear absorber acting on a nonlinear host structure are reported. Section 5 then carries out the experimental demonstration of the digital nonlinear absorber for which different nonlinear (polynomial) laws are considered. Finally, the conclusions of the present study are drawn in Section 6.

2. Piezoelectric tuned vibration absorbers

2.1. Linear piezoelectric tuned vibration absorber

A resonant shunt circuit comprises an inductor and a resistor, arranged either in series or in parallel. Figure 1 depicts a single-degree-of-freedom (SDOF) mechanical oscillator with a piezoelectric stack connected to a series RL shunt circuit.

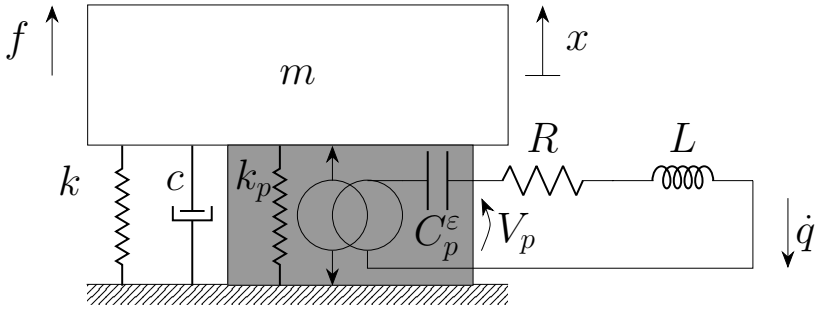

Figure 1: Mechanical oscillator with a piezoelectric transducer shunted by a series RL circuit.

The system is governed by the following equations [2]

$$\begin{cases} m\ddot{x} + c\dot{x} + k_{oc}x - \theta q &= f \\ L\ddot{q} + R\dot{q} &= V_p \end{cases}, \tag{1}$$

where the voltage across the piezoelectric transducer V_p is given by

$$V_p = \theta x - \frac{q}{C_p^\varepsilon}, \tag{2}$$

Parameters m and c are the mass and damping of the SDOF oscillator, respectively, $k_{oc} = k + k_p$ is the total structural stiffness (with k the stiffness of the structure without piezoelectric transducer, and k_p the stiffness of the piezoelectric transducer when it is open-circuited), x is the displacement of the mechanical oscillator, θ is a coupling coefficient, f is the external forcing, L and R are the inductance and resistance of the shunt circuit, respectively, C_p^ε is the piezoelectric capacitance at constant strain and q is the electrical charge flowing through the piezoelectric transducer. An upper dot denotes time derivation.

The shunt circuit parameters can be tuned in a number of ways according to the objectives at hand, see, e.g., the recent paper by Ikegame et al [4]. Because this study considers harmonic forcing, the H_∞-optimum tuning given by Soltani et al [3] is adopted. The generalized electromechanical coupling factor K_c is given by [2]

$$K_c^2 = \frac{\omega_{oc}^2 - \omega_{sc}^2}{\omega_{sc}^2}, \tag{3}$$

where ω_{sc} and ω_{oc} are the angular resonance frequencies of the structure when the piezoelectric transducer is short-circuited and open-circuited, respectively. An intermediate variable r is introduced as

$$r = \frac{\sqrt{64 - 16K_c^2 - 26K_c^4} - K_c^2}{8}, \tag{4}$$

which is related to the equal-peak amplitude h through $h = (1+K_c^2)/(k_{oc}\sqrt{1-r^2})$. The optimal inductance and resistance values are then given by

$$L = \frac{4K_c^2 + 4}{3K_c^2 - 4r + 8} \frac{1}{\omega_{oc}^2 C_p^\varepsilon} \tag{5}$$

and

$$R = \frac{2\sqrt{2\left(K_c^2+1\right)\left(27K_c^4 + K_c^2(80-48r) - 64(r-1)\right)}}{\left(5K_c^2+8\right)\sqrt{3K_c^2 - 4r + 8}} \frac{1}{\omega_{oc} C_p^\varepsilon}, \tag{6}$$

respectively [3, 4]. For illustration, considering the linear parameters of the experimental set-up described in Section 4 and listed in Table 1, the PTVA parameters in Table 2 are obtained. Eventually, this tuning methodology yields the so-called *equal-peak design*, as illustrated in Figure 2.

2.2. Nonlinear piezoelectric vibration absorber

When the host structure is nonlinear, a linear PTVA can quickly become detuned due to its narrow bandwidth. The purposeful introduction of nonlinearity in the PTVA and the subsequent harnessing of its behavior allows the absorber to remain tuned to the changing frequency of the host structure [15]. For this purpose, the functional form of

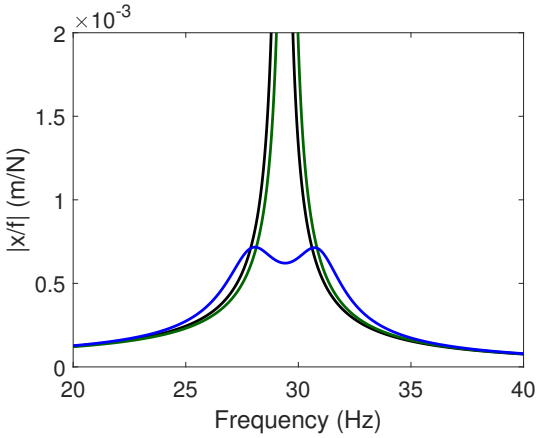

Figure 2: Frequency response function of the system in Figure 1: short-circuited piezoelectric transducer (—), open-circuited piezoelectric transducer (—) and equal-peak design (—).

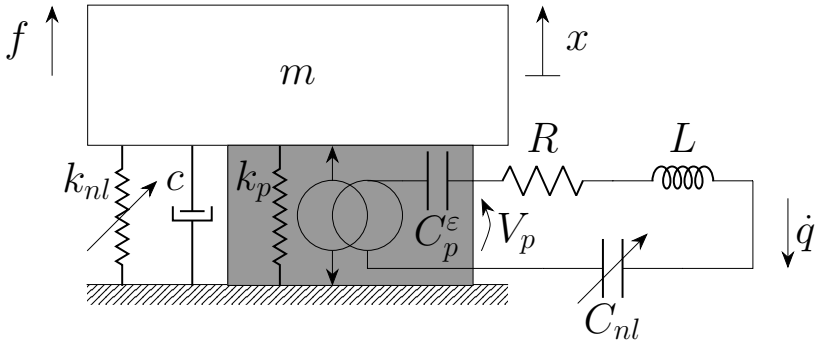

Figure 3: Nonlinear oscillator with a piezoelectric transducer shunted by a series RL circuit possessing a nonlinear capacitor.

the nonlinearity in the PTVA is to be chosen according to a *principle of similarity* [22], i.e., it should be identical to that of the host structure.

For a nonlinear shunt circuit coupled to a Duffing oscillator, depicted in Figure 3, the governing equations read

$$\begin{cases} m\ddot{x} + c\dot{x} + k_{oc}x + k_3x^3 - \theta q &= f \\ L\ddot{q} + R\dot{q} + C_3q^3 &= V_p \end{cases} \tag{7}$$

where k_3 is the cubic stiffness coefficient and C_3 is the cubic capacitance coefficient ($C_3 = 0$ for a linear shunt circuit) [12]. This latter coefficient can be determined from the parameters of the system using the simplified formula in [18]:

$$C_3 = \frac{2L^2}{m^2}k_3, \tag{8}$$

Figure 4 shows the nonlinear frequency responses (NFRs) of the Duffing oscillator controlled by either a linear (Figure 4a) or nonlinear (Figure 4b) PTVA. These responses were computed using a harmonic balance formalism coupled with a continuation

procedure [23]. As the forcing amplitude increases, the linear absorber becomes severely detuned, which generates detrimental vibrations. Conversely, the nonlinear PTVA performance remains unchanged for the different forcing amplitudes.

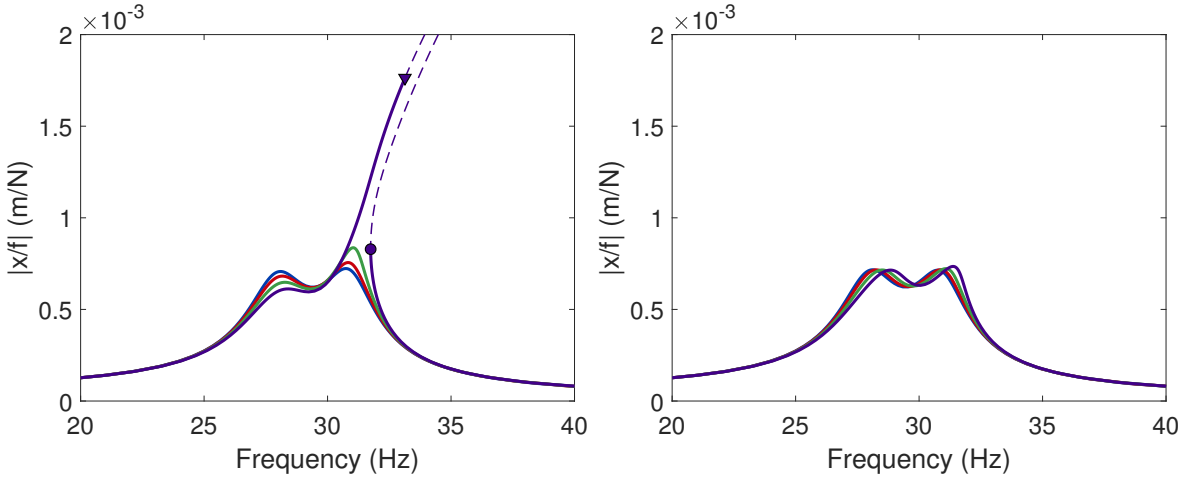

Figure 4: NFRs of a Duffing oscillator controlled by a linear (a) and nonlinear (b) PTVA: 0.2N (—), 0.4N (—), 0.6N (—), 0.8N (—). —: stable solution, - - : unstable solution, ● : fold bifurcation, ▼: Neimark-Sacker bifurcation.

3. A digital piezoelectric vibration absorber

When it comes to the practical realization of a PTVA, a number of challenges have to be overcome. The first difficulty is the large inductance value (typically hundreds of Henries) required for structures with low resonance frequencies. Although physical inductors with such high inductance values were realized [24], they are not commercially available. A common workaround is to use synthetic inductors or gyrators, but they come with non-ideal characteristics, such as frequency-dependent resistance [25]. Another challenge pertaining to nonlinear absorbers is the tailoring of the nonlinear behavior of the electrical components so as to obey the principle of similarity. Even if this problem was addressed for cubic nonlinearities through the use of saturable inductors [18], there is not much variety in the functional forms that can be realized with electrical components.

The concept of synthetic impedance proposed by Fleming et al [21] solves these issues altogether. A digital signal processing unit together with a current source make the realization of an arbitrary impedance possible. This however comes at the expense of a non-fully-passive absorber (because the analog and digital electronics need power) and at the risk of creating instabilities (because the system contains active elements). The realization of a synthetic impedance mimicking a PTVA is discussed in what follows.

3.1. Hardware

The digital vibration absorber used in this study comprises two parts, namely a digital processing unit and an analog board. The digital processing unit implements the desired input-output (I/O) relation between the voltage across the electrodes of the piezoelectric transducer and its current. The analog board serves as the interface between the piezoelectric transducer and the digital processing unit.

The schematic of the digital absorber is depicted in Figure 5. It is very similar to that used by Matten et al [26]. The patch voltage V_p is measured with a voltage divider made of R_1 and R_2. The operational amplifier OA1 is a follower [27] which outputs a fraction of the patch voltage αV_p, where $\alpha = R_2/(R_1 + R_2)$. A constant offset voltage ΔV_{in} is generated by a shunt voltage regulator to comply with the input voltage range of the analog-to-digital converter (ADC) of the microcontroller unit (MCU). OA2 sums the two voltages and outputs $\alpha V_p + \Delta V_{in}$. The MCU computes the input-output relation to inject the desired current and sends a voltage signal with its digital-to-analog converter (DAC) to OA3, whose output simply follows the input. Since the output voltage range of the MCU may not be symmetric with respect to the circuit ground, another offset voltage ΔV_{out} is generated by a shunt voltage regulator. OA4 subtracts this offset to the output of OA3. This results in an output voltage signal V_{out} proportional to the current to be injected in the transducer. This voltage signal is imposed on one pole of the resistor R_i, while the other one is maintained to a virtual ground by OA5. Thus, the current injected into the piezoelectric patch is V_{out}/R_i.

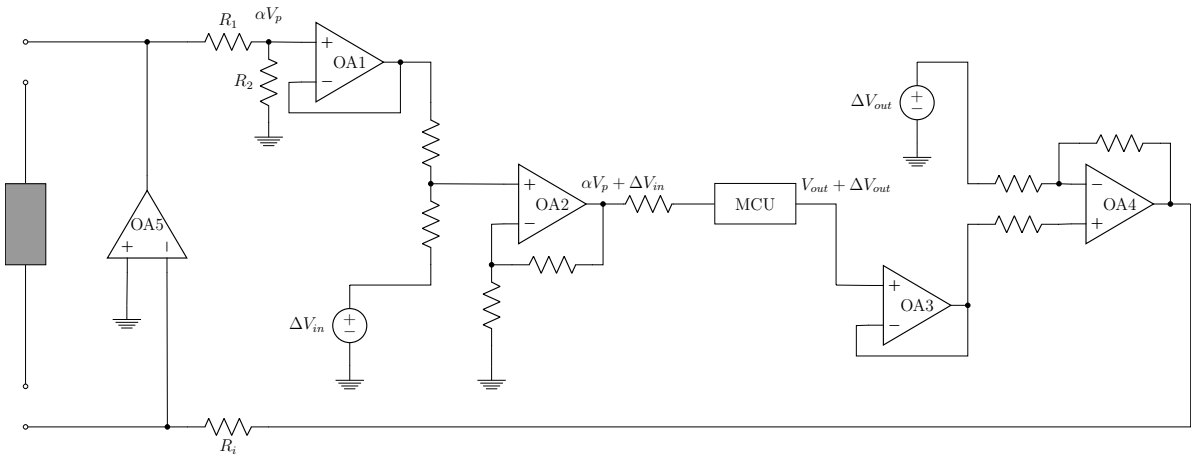

Figure 5: Layout of the digital absorber. The gray box represents the piezoelectric transducer.

The MCU used in this work is an Arduino Due. This microcontroller was chosen for its price, availability, ease to use and the presence of DACs. The operational amplifier OA5, a PA78 power operational amplifier from APEX Microtechnology [28], is able to cope with the high voltages generated by the piezoelectric transducer, which went up to ± 150V.

3.2. Software

The Arduino Due can easily be programmed to implement an arbitrary I/O relation with MATLAB Simulink. The I/O relation may be represented as a block diagram, and the support packages for Arduino Hardware were used to generate the code to be uploaded to the microcontroller in a fully automated way.

3.2.1. Linear PTVA Implementing a linear PTVA is fairly straightforward, as depicted in Figure 6. The ADC reads a voltage level and translates it into an unsigned integer number. This integer is reconverted to a floating point number representing a voltage level by the gain g_{in}. An offset ΔV_{in} is added to compensate for the input voltage offset generated by the analog board. The shifted and scaled signal is processed according to the desired I/O relation Y, the synthesized shunt circuit admittance [21]. It is then amplified by a gain g whose purpose is explained hereafter. The output signal is passed through a saturation operator to avoid integer overflow at the DAC. Finally, the output signal is shifted (by ΔV_{out}) and scaled (by g_{out}) back to an unsigned integer to be fed to the DAC.

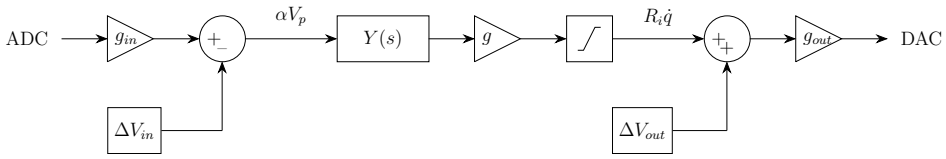

Figure 6: Block diagram of the synthesized linear PTVA.

If properly tuned, every voltage offset from the analog board should be compensated by an offset in the software. The remaining parameter to tune is the gain g whose purpose is to ensure the consistency of the I/O relation with a shunt circuit from the point of view of the transducer. If the offsets are perfectly compensated, the current $i = \dot{q}$ injected into the transducer should be

$$i(s) = \frac{1}{R_i} V_{out}(s) = \frac{g\alpha}{R_i} Y(s) V_p(s), \tag{9}$$

where s is the Laplace variable. Equation (9) shows that if the emulated shunt circuit is to mimic the desired admittance, the following consistency condition should be ensured

$$\frac{g\alpha}{R_i} = 1 \tag{10}$$

3.2.2. Nonlinear PTVA The nonlinear voltage can be computed if the charge flowing through the piezoelectric transducer is known. It can be retrieved from the output voltage since

$$V_{out} = R_i \dot{q} \tag{11}$$

Moreover, using Kirchhoff's voltage law,

$$\alpha V_p = \alpha V_L + \alpha V_{NL}, \tag{12}$$

where $V_L = L\ddot{q} + R\dot{q}$ is the voltage across the RL circuit and $V_{NL} = C_3 q^3$ is the voltage across the nonlinear capacitor. Then, Equation (11) and Equation (12) suggest that the nonlinear shunt circuit may be implemented by adding a nonlinear feedback [29] to the block diagram in Figure 6, as depicted in Figure 7.

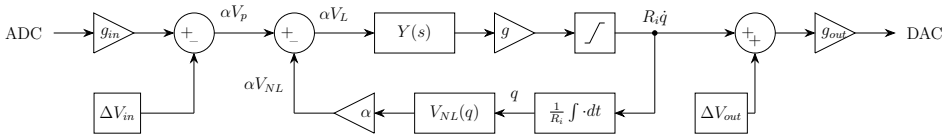

Figure 7: Block diagram of the synthesized nonlinear PTVA.

Small signal offsets are unavoidable in practice. This causes a drift of the integrator and an eventual saturation of the signals. As a remedy, a lossy integrator (i.e., a first-order lowpass filter) or a bandpass filter can replace the integrator. The passband of such filters should be in a low frequency range, such that the filter behaves as an integrator in the frequency range of interest. The advantage of using a bandpass filter over a lossy integrator is its ability to completely reject DC offsets, preventing asymmetric AC signal distortion.

4. Experimental demonstration of a digital linear PTVA

4.1. Experimental setup

The structure under investigation is a clamped-free beam with a clamped thin lamina attached to its free end, as shown in Figure 8. Due to its large relative deformation, the thin lamina causes an overall hardening nonlinear structural behavior, which can accurately be modeled using a cubic spring. The structure is excited near its free end by an electrodynamic shaker (TIRA TV 51075). An impedance head (DYTRAN 5860B) is used to measure the force applied to the structure and the corresponding acceleration. The measurements are recorded by an acquisition system (LMS Scadas Mobile).

The beam is covered over its whole length with ten cells, composed of pairs of stacks of two PSI-5A4E piezoelectric patches, each pair being placed on either side of the beam. The five cells closest to the clamped end are connected in parallel and used for mitigating the resonant vibrations around the first beam mode, whereas the five other cells are left in open circuit. More details about the experimental setup can be found in [18].

The digital absorber connected to the patches is powered by a high-voltage (HV) power supply with ±150V (to power the operational amplifier OA5 in Figure 5) and with a low-voltage (LV) power supply with ±10V (to power the interface with the microcontroller unit). The microcontroller is programmed and powered via USB.

The voltage division ratio $\alpha = 0.0109$ was set so that a maximum input voltage at the MCU (± 1.65V) corresponds nearly to a maximum output voltage of OA5 (± 150V). The current injector resistance R_i=152.9Ω was measured with a multimeter (FLUKE

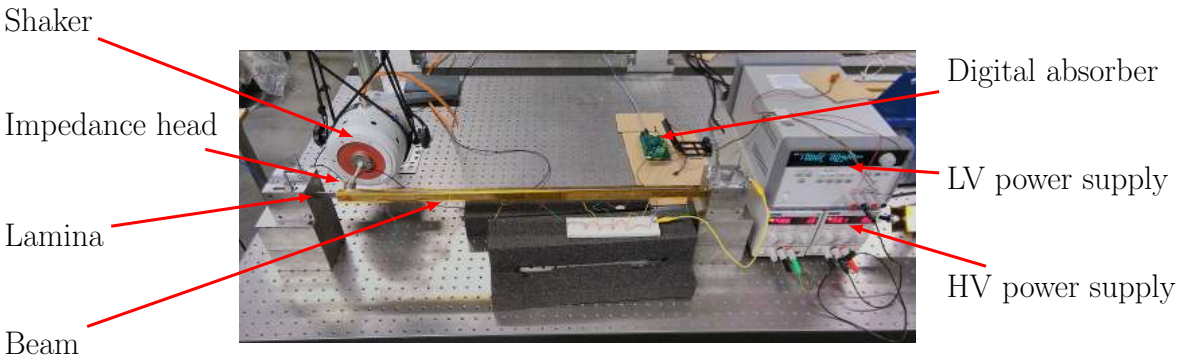

Figure 8: Picture of the experimental setup.

177). The gain $g = 14,021$ was deduced from Equation (10). The voltage offsets ΔV_{in} and ΔV_{out} were both set to 1.65V, so that the full ADC and DAC ranges of the MCU could be used.

4.2. System identification

The first step to tune the shunt circuit is to identify the parameters of the host system. The piezoelectric capacitance was measured with a multimeter (FLUKE 177). The linear mechanical parameters were determined from a low-level broadband excitation. A first test was performed with open-circuited patches ($q = 0$). The obtained frequency response function (FRF) was fitted to obtain a minimum least-squares error between the model and the measurements, giving an estimate of the parameters m, c and k_{oc}. The process was repeated with short-circuited patches, giving an estimation of k_{sc}, the structural stiffness when the piezoelectric patches are short-circuited ($V_p = 0$). From Equation (1) and Equation (2), it can be derived that the following relation holds:

$$k_{sc} = k_{oc} - \theta^2 C_p^{\varepsilon} \tag{13}$$

so that θ can be deduced from the estimated quantities. The system has a generalized electromechanical coupling factor K_c=12.43%. Table 1 contains the identified parameters. Figure 9 shows an excellent agreement between the experimental and predicted FRFs.

The nonlinear stiffness of the thin lamina was estimated by exciting the system with short-circuited patches at higher forcing amplitudes. The excitation was a stepped sine with a controlled amplitude of 0.2N between 28 and 32Hz. Following [18], the recorded force and acceleration signals were digitally bandpass filtered and gathered in vectors $\mathbf{f}$ and $\ddot{\mathbf{x}}$, respectively. The velocity and displacement vectors were estimated by time integration. Rewriting the first line of Equation (7)

$$\mathbf{x}^3 k_3 = \mathbf{f} - [\ddot{\mathbf{x}}, \dot{\mathbf{x}}, \mathbf{x}] \begin{bmatrix} m \\ c \\ k_{sc} \end{bmatrix} \tag{14}$$

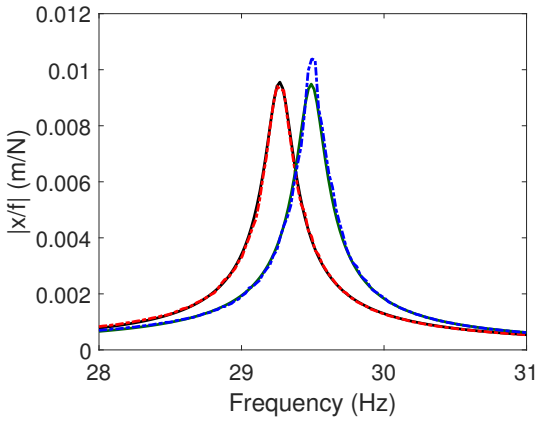

Figure 9: Experimental and predicted FRFs: model (sc: —, oc: —) and measurements (sc: -·-, oc: -·-).

Table 1: Identified parameters of the experimental setup.

Characteristic	m (kg)	c (Ns/m)	k_{sc} (N/m)	k_{oc} (N/m)	k_3 (N/m^3)	C_p^{ε} (nF)	θ (N/C)
Value	0.4464	0.5690	1.4975×10^4	1.5207×10^4	2.5046×10^9	250	3.04248×10^4

shows that the nonlinear force vector $\mathbf{x}^3 k_3$ can be calculated from the knowledge of the linear parameters at each time instant. It is represented by the black dots in Figure 10. Eventually, the nonlinear coefficient k_3 in Table 1 was identified through simple least-squares fitting of the nonlinear force with a cubic law.

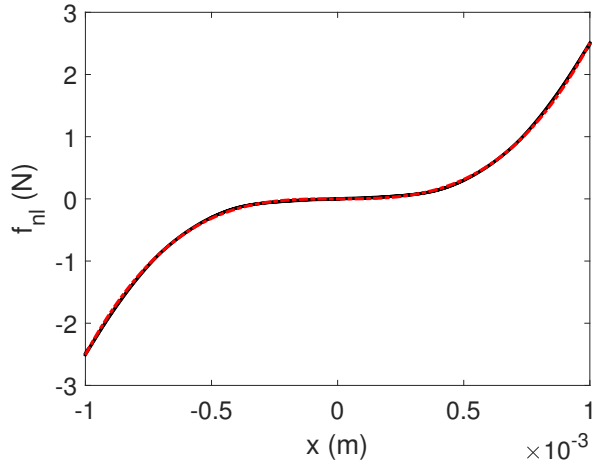

Figure 10: Nonlinear stiffness curve: measurement (•) and fitted cubic law (-·-).

4.3. Synthesized admittance

Based on the previous system identification, the parameters of the digital linear PTVA in Table 2 were computed using Equation (5) and Equation (6). The slight variability

Table 2: Parameters of the linear and nonlinear PTVAs.

Parameter	L (H)	R (Ω)	C_3 (V/C^3)
Value	117.42	3 295	3.4022×10^{14}

of the results from one test to another led to adaptations of the inductance L of the order of 1% of the theoretical value. This adaptation was carried out to obtain equal peaks at the lowest forcing amplitude, namely f=0.2N. The shunt circuit admittance was synthesized in the MCU after transforming the continuous admittance

$$Y(s) = \frac{1}{Ls + R} \tag{15}$$

into a discrete transfer function using Tustin's method. The sampling frequency of the MCU was 10kHz.

The input and output signals were measured by the MCU and recorded by a computer. The piezoelectric charge and current time derivative were estimated offline by time integration and time derivation of the output signal, respectively. Figure 11 and Figure 12, which compare the theoretical and post-processed voltages across the resistor and inductor, respectively, confirm that the MCU implements the desired input-output transfer function.

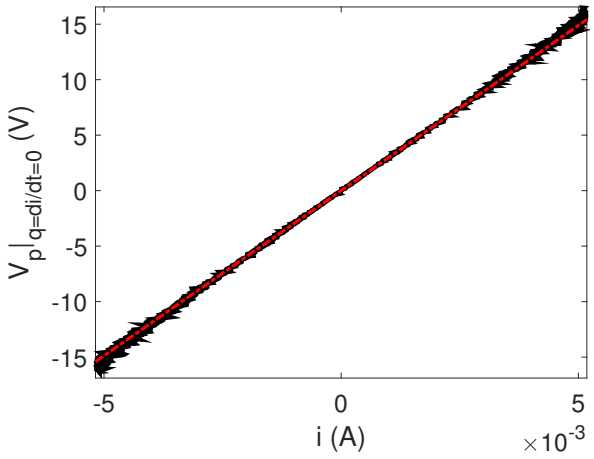

Figure 11: Voltage across the resistor: theoretical law (-·-) and measurements (•).

4.4. Performance of the linear PTVA

The experimental NFRs for forcing levels ranging from 0.2N to 0.8N are presented in Figure 13a. At 0.2N, the nonlinearity of the thin lamina is not activated; the linear PTVA gives rise to two equal peaks in the response. As the forcing level is increased, a clear detuning of the linear PTVA is observed. The comparison with the theoretical NFRs in Figure 4a reveals that the detuning is in fact more important than predicted.

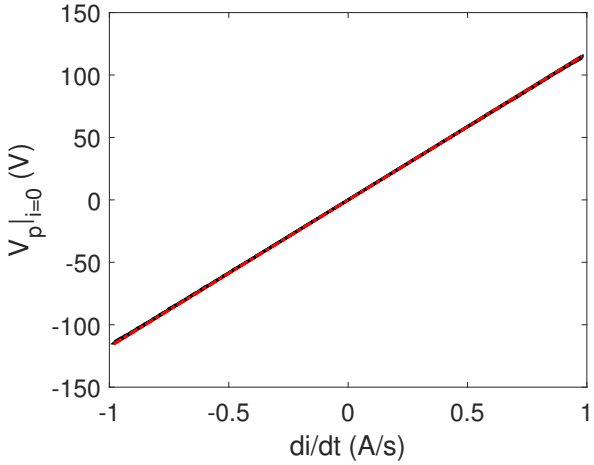

Figure 12: Voltage across the inductor: theoretical law (-·-) and measurements (•).

After detailed investigations, this detuning was attributed to the nonlinear behavior of the piezoelectric patches, as in [18]. The model in Equation (2) was thus upgraded using a negative cubic capacitance $C_{p,3}$ and a positive cubic resistance $R_{p,3}$, so that

$$V_p = \theta x - \frac{1}{C_p^{\varepsilon}} q - C_{p,3} q^3 - R_{p,3} \dot{q}^3, \tag{16}$$

with values given in Table 3. The NFRs predicted through this updated model in Figure 13b are now in close agreement with the experimental NFRs in Figure 13a.

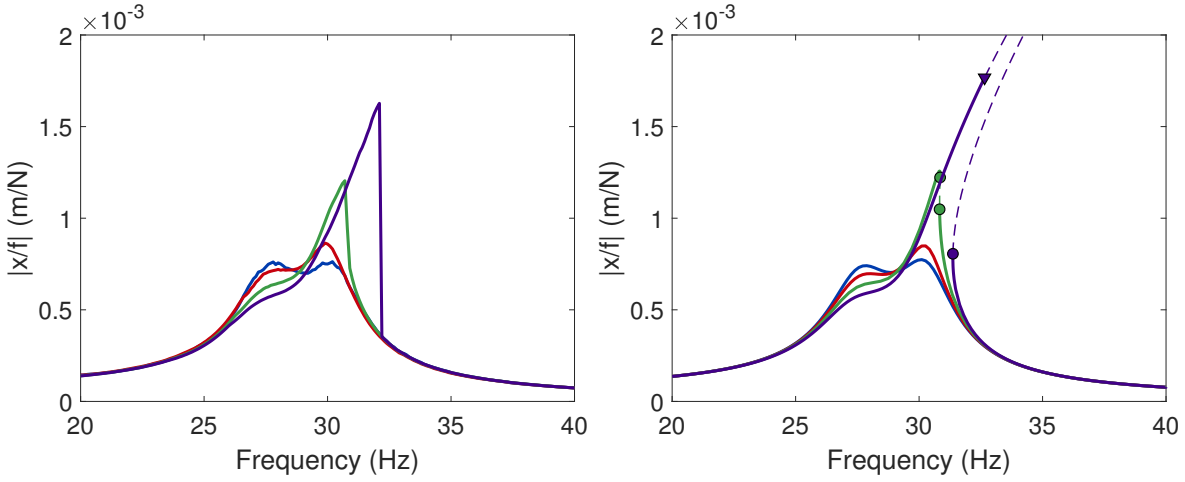

Figure 13: Experimental (a) and theoretical (updated) NFRs (b) of the nonlinear beam with a digital linear PTVA: 0.2N (—), 0.4N (—), 0.6N (—), 0.8N (—). —: stable solution, - - : unstable solution, ● : fold bifurcation, ▼: Neimark-Sacker bifurcation.

Table 3: Identified nonlinear parameters of the piezoelectric transducer.

Characteristic	$C_{p,3}$ (V/C^3)	$R_{p,3}$ (V/A^3)
Value	-2.3629×10^{14}	1.5352×10^7

5. Experimental demonstration of a digital nonlinear PTVA

5.1. Synthesized admittance

To address the detuning of the linear PTVA in nonlinear regimes of motion, a cubic capacitance was introduced in the synthetic admittance (αV_{NL} in Figure 7). Accounting for the nonlinear behavior of the piezoelectric transducer, the value of the nonlinear capacitance was calculated to be $C_3 - C_{p,3} \approx 1.7C_3$. The measured voltage of the nonlinear capacitor in Figure 14 was found to closely follow the law prescribed by the design.

We note that, to fully comply with the theoretical work of [15], a negative cubic resistance should also have been added to the synthesized shunt circuit to compensate for the positive cubic resistance in Equation (16), but this was avoided to prevent any risk of instability caused by such an active component. The linear resistance was nevertheless diminished by 10% in an attempt to limit the dissipation in the circuit at high forcing amplitudes. As shall be shown in Subsection 5.4, this has a limited impact on the performance of the digital nonlinear PTVA at low forcing levels.

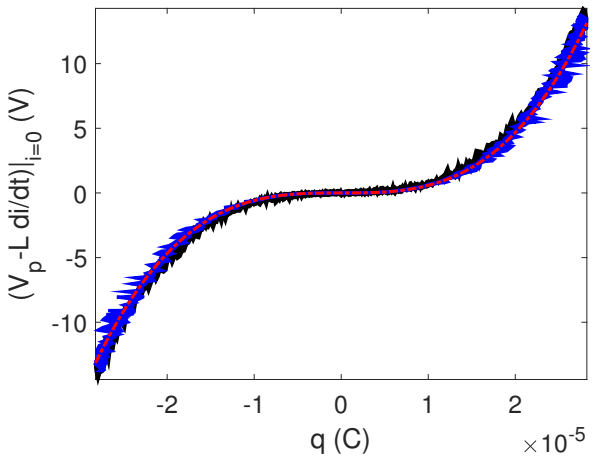

Figure 14: Voltage across the nonlinear capacitor: theoretical law (-·-), direct measurements of V_{nl} (•) and post-processed measurements from the input and output signals (•).

5.2. Performance of the nonlinear PTVA

Figure 15a displays the experimental NFRs for forcing levels ranging from 0.2N to 0.8N. Clearly, the nonlinear PTVA is able to maintain equal peaks in the frequency response for all forcing levels considered, confirming its superior performance over its linear counterpart. Furthermore, these experimental curves are in excellent agreement with the theoretical NFRs in Figure 15b.

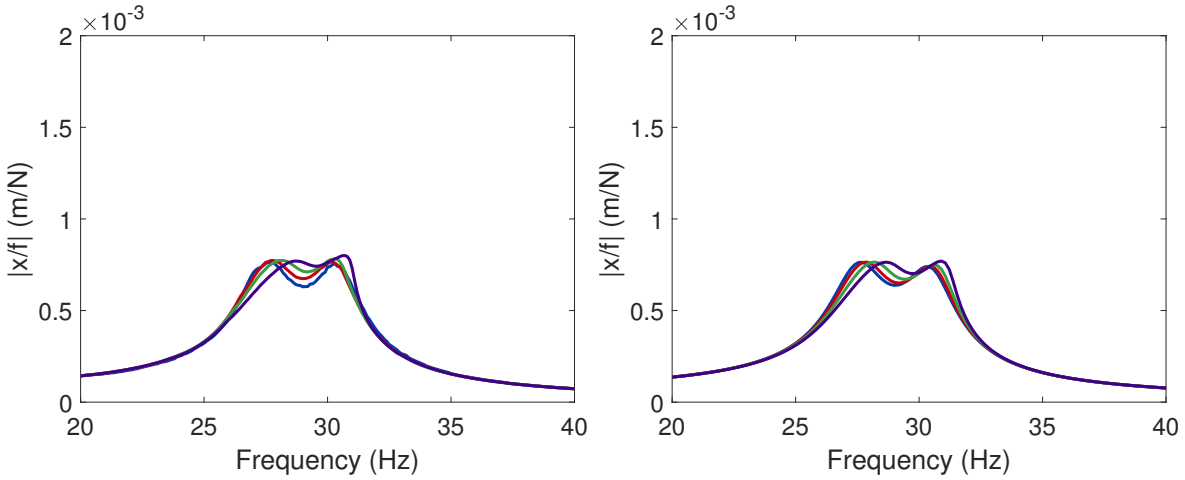

Figure 15: Experimental (a) and theoretical NFRs (b) of the nonlinear beam with a digital nonlinear PTVA: 0.2N (—), 0.4N (—), 0.6N (—), 0.8N (—).

A series of tests at higher forcing amplitudes was performed to investigate the potentially adverse dynamics brought by the nonlinear PTVA. Because of the detuning of the linear PTVA, these tests were not performed with this latter absorber in order to avoid the rupture of the thin lamina. Figure 16a depicts that the nonlinear PTVA starts to be slightly detuned at 1N, with a more pronounced detuning at 1.2N. The theoretical response in Figure 16b indicates that a detached resonance curve merges with the main response, marking the end of the working range of the nonlinear PTVA [15].

The digital nonlinear PTVA suffers from another limitation depicted in Figure 17. At 1.2N, the input signal of the MCU reaches its saturation limits, meaning that the operational amplifier OA5 in Figure 5 saturates correspondingly. The output signal saturates as well. This issue can be resolved by decreasing R_i, thereby decreasing g by virtue of Equation (10), and thus the magnitude of the output signal, but this was not attempted in this work since the input voltage saturates anyway.

5.3. Validation of the principle of similarity

Quadratic, $C_2\text{sign}(q)q^2$, and quintic, C_5q^5, nonlinear capacitances were also considered separately in the MCU. After fitting the cubic nonlinear restoring force of the thin lamina with quadratic and quintic laws, as shown in Figure 18, the coefficient of the

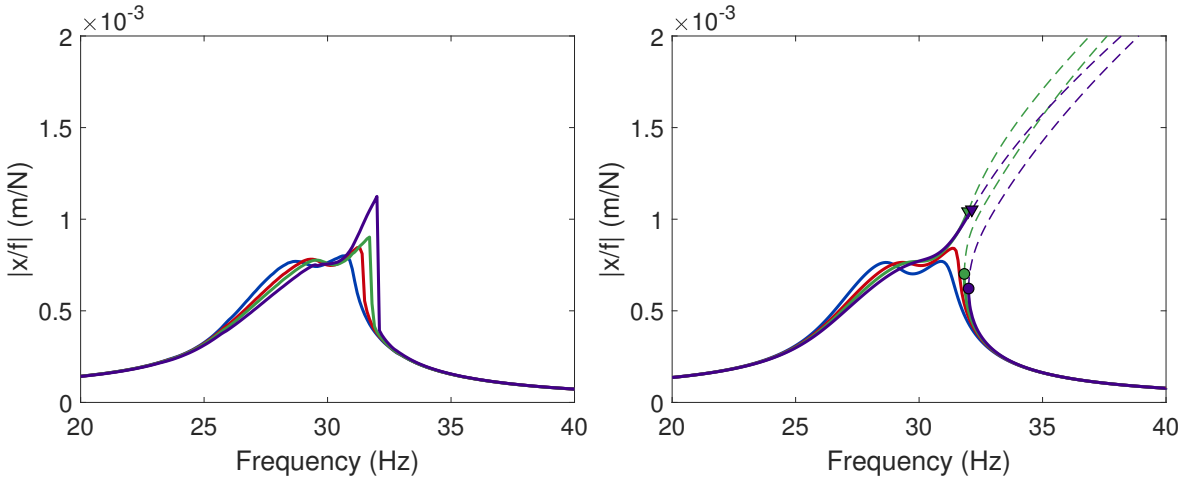

Figure 16: Experimental NFRs (a) and theoretical NFRs (b) of the nonlinear beam with a digital nonlinear PTVA: 0.8N (—), 1.0N (—), 1.1N (—), 1.2N (—). —: stable solution, - - : unstable solution, ● : fold bifurcation, ▼: Neimark-Sacker bifurcation.

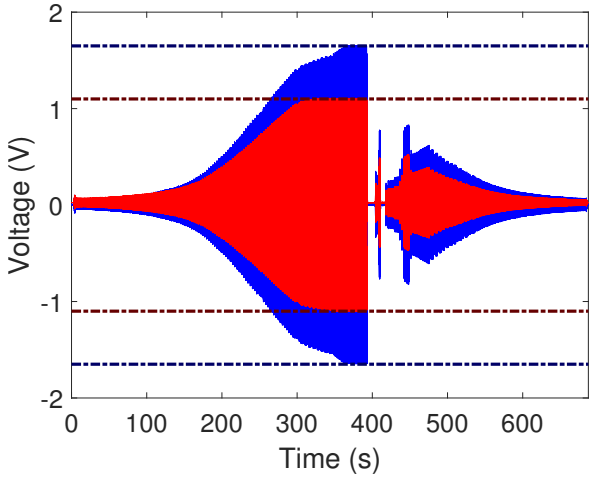

Figure 17: Signals recorded in the MCU for a nonlinear PTVA at f=1.2N: input voltage (—) and its saturation limits at ±1.65V (-·-), output voltage (—) and its saturation limits at ±1.1V (-·-).

nonlinear capacitance was computed based on this assumed restoring force using the formulas from [22].

Figure 19 displays the corresponding NFRs. In both cases, a clear detuning is observed compared to Figure 15, which confirms the fact that a cubic capacitance is the optimal choice for a cubic nonlinearity in the host structure, which, in turn, validates the adopted principle of similarity. The detuning can be understood from Figure 18, where the stiffness is first overestimated (resp. underestimated) and then underestimated (resp. overestimated) for a quadratic (resp. quintic) nonlinearity, leading to the same trend for the absorber frequency.

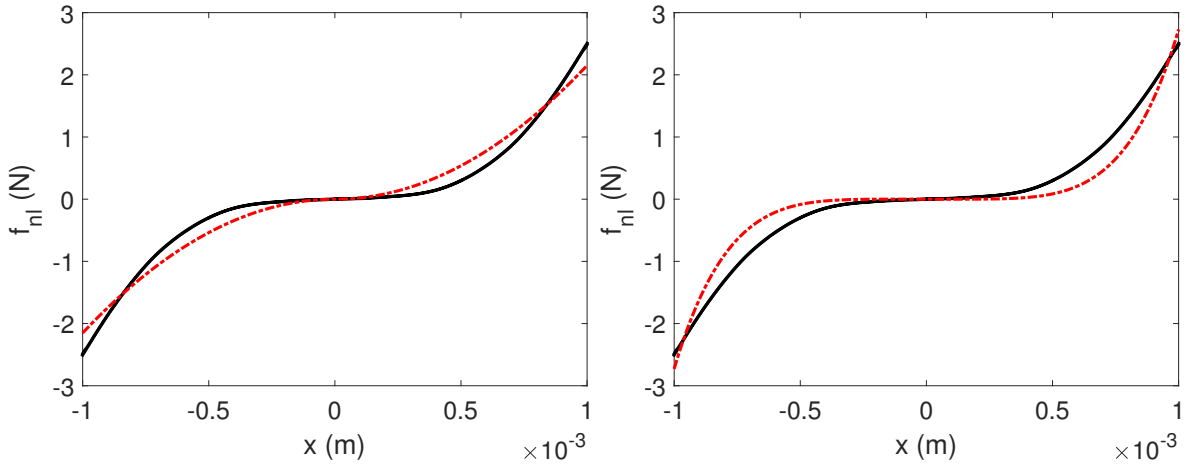

Figure 18: Fitting the cubic nonlinearity of the thin lamina with a quadratic (a) or a quintic (b) nonlinearity: measurements (•) and fitted model (- - -).

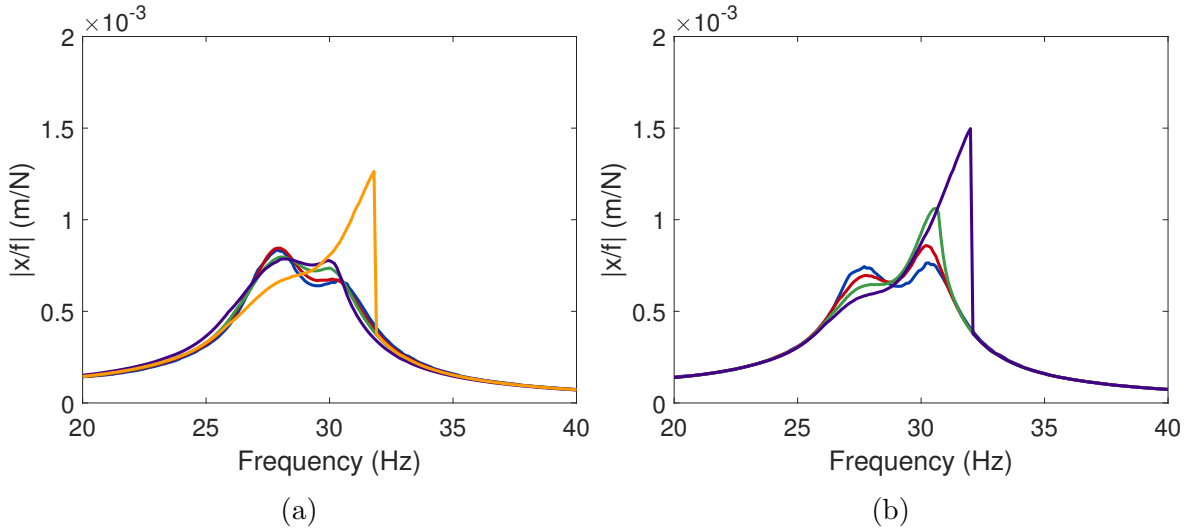

Figure 19: Experimental NFRs of the nonlinear beam with a digital PTVA with quadratic (a) or quintic (b) capacitance: 0.2N (—), 0.4N (—), 0.6N (—), 0.8N (—), and 1.0N (—).

5.4. Parametric study

Given the ease with which the parameters of a digital absorber can be modified, performing a parametric study was relatively straightforward. A first parametric study was carried out at a low-level excitation (0.2N). In Figure 20, the great sensitivity with respect to the inductance is visible, as a 5% change leads to a 30% relative difference in maximum amplitude. Figure 21 shows that the sensitivity on the resistance is much less pronounced. As announced in Subsection 5.2, decreasing the resistance by 10% has almost no effect on the maximum amplitude.

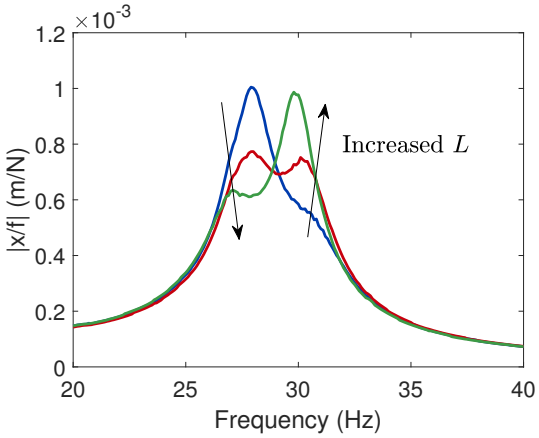

Figure 20: Experimental NFRs of the nonlinear beam with a nonlinear PTVA at f=0.2N when the nominal inductance is multiplied by 0.95 (—), 1.0 (—) and 1.05 (—).

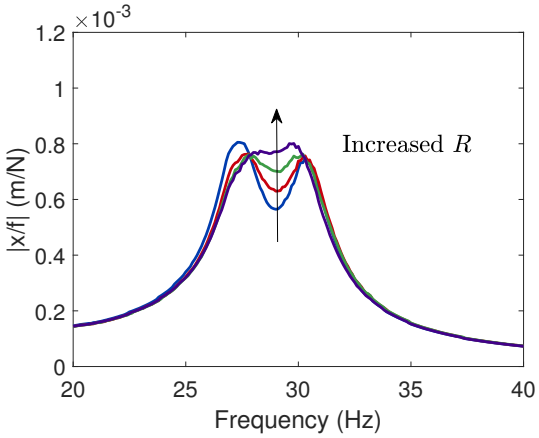

Figure 21: Experimental NFRs of the nonlinear beam with a nonlinear PTVA at f=0.2N when the nominal resistance is multiplied by 0.8 (—), 0.9 (—), 1.0 (—) and 1.1 (—).

A second parametric study was performed at 0.6N. Figure 22 shows that the nominal nonlinear capacitance (i.e., without the correction for the nonlinearity of the piezoelectric transducer) cannot enforce equal peaks. It is only when the nominal value is multiplied by 2 that equal peaks are obtained. A too large nonlinear capacitance is also detrimental to performance. When comparing Figure 20 and Figure 22, we see that the relative changes in inductance value give rise to much higher detuning than the same relative change in the value of the capacitance.

Finally, Figure 23 shows what happens when the resistance is varied in a nonlinear regime of motion. Qualitatively, the conclusions are the same as in Figure 21, although quantitatively, an increased resistance appears to hinder more the damping ability of the shunt circuit in nonlinear regimes of motion.

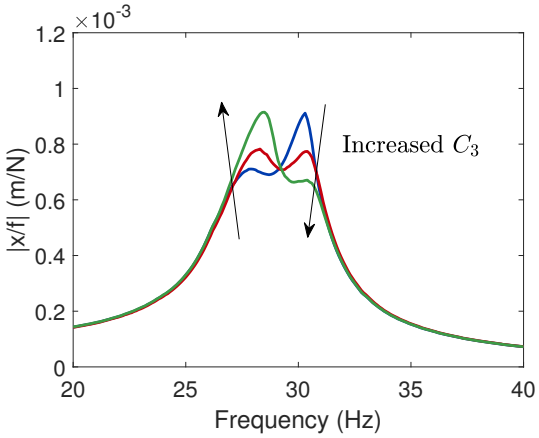

Figure 22: Experimental NFRs of the nonlinear beam with a nonlinear PTVA at f=0.6N when the nominal nonlinear capacitance is multiplied by 1.0 (—), 2.0 (—) and 3.0 (—).

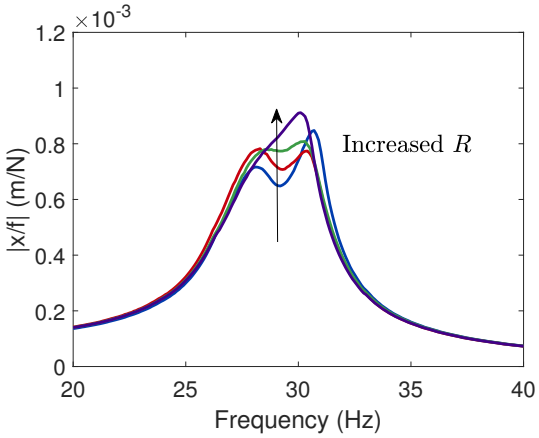

Figure 23: Experimental NFRs of the nonlinear beam with a nonlinear PTVA at f=0.6N when the nominal resistance is multiplied by 0.8 (—), 0.9 (—), 1.0 (—) and 1.1 (—).

6. Conclusion

This study presented a digital piezoelectric tuned vibration absorber. Due to its inherent flexibility, this absorber can synthesize linear and nonlinear shunt circuits (with arbitrary mathematical forms for the nonlinearity). The experimental demonstration on a structure with hardening nonlinear behavior showed the superiority of the digital nonlinear absorber over its linear counterpart. It also served to validate the adopted principle of similarity.

This work constitutes a step toward the implementation of absorbers able to effectively mitigate the vibrations of real-life, nonlinear structures. In this framework, digital absorbers constitute an attractive solution, as they are easy to program and to fine-tune. Future works may involve the generalization of this absorber to make it able to control multiple nonlinear structural resonances.

Acknowledgments

The authors would like to acknowledge the financial support of the SPW (WALInnov grant 1610122).

References

[1] Forward R L 1979 *Applied Optics* **18** 690 ISSN 0003-6935 URL https://www.osapublishing.org/abstract.cfm?URI=ao-18-5-690

[2] Hagood N and von Flotow A 1991 *Journal of Sound and Vibration* **146** 243–268 ISSN 0022460X URL https://linkinghub.elsevier.com/retrieve/pii/0022460X91907629

[3] Soltani P, Kerschen G, Tondreau G and Deraemaeker A 2014 *Smart Materials and Structures* **23** 125014 ISSN 0964-1726 URL http://stacks.iop.org/0964-1726/23/i=12/a=125014?key=crossref.798743ce34b627bed945b046d8a6b51a

[4] Ikegame T, Takagi K and Inoue T 2019 *Journal of Vibration and Acoustics* **141** 031015 ISSN 1048-9002 URL http://vibrationacoustics.asmedigitalcollection.asme.org/article.aspx?doi=10.1115/1.4042819

[5] Gripp J and Rade D 2018 *Mechanical Systems and Signal Processing* **112** 359–383 ISSN 08883270 URL https://doi.org/10.1016/j.ymssp.2018.04.041 https://linkinghub.elsevier.com/retrieve/pii/S0888327018302437

[6] Den Hartog J P 1985 *Mechanical vibrations* (Courier Corporation) ISBN 0070163898

[7] Fahy F and Schofield C 1980 *Journal of Sound and Vibration* **72** 365–378 ISSN 0022460X URL https://linkinghub.elsevier.com/retrieve/pii/0022460X80903831

[8] Khavasi A 2015 *Journal of the Optical Society of America B* **32** 1941 ISSN 0740-3224 URL https://www.osapublishing.org/abstract.cfm?URI=josab-32-9-1941

[9] Arsanjani A, Biabanifard M and Abrishamian M S 2019 *Superlattices and Microstructures* **128** 157–169 ISSN 07496036 URL https://doi.org/10.1016/j.spmi.2019.01.020 https://linkinghub.elsevier.com/retrieve/pii/S074960361831989X

[10] Biabanifard M and Abrishamian M S 2018 *Applied Physics A: Materials Science and Processing* **124** 826 ISSN 14320630 URL http://link.springer.com/10.1007/s00339-018-2248-3

[11] Hui Y, Gomez-Diaz J S, Qian Z, Alù A and Rinaldi M 2016 *Nature Communications* **7** 11249 ISSN 2041-1723 URL http://www.nature.com/articles/ncomms11249

[12] Agnes G S and Inman D J 1996 *Smart Materials and Structures* **5** 704–714 ISSN 0964-1726 URL http://stacks.iop.org/0964-1726/5/i=5/a=018?key=crossref.1ae9e6cd0aa97b0ac65119847b1ad283

[13] Richard C, Guyomar D, Audigier D and Bassaler H 2000 Enhanced semi-passive damping using continuous switching of a piezoelectric device on an inductor vol 3989 ed Hyde T T pp 288–299 ISSN 0277786X URL http://proceedings.spiedigitallibrary.org/proceeding.aspx?articleid=924877

[14] Zhou B, Thouverez F and Lenoir D 2014 *Journal of Sound and Vibration* **333** 2520–2542 ISSN 0022460X URL http://dx.doi.org/10.1016/j.jsv.2013.12.019 https://linkinghub.elsevier.com/retrieve/pii/S0022460X13010596

[15] Soltani P and Kerschen G 2015 *Smart Materials and Structures* **24** 075015 ISSN 0964-1726 URL http://dx.doi.org/10.1088/0964-1726/24/7/075015 http://stacks.iop.org/0964-1726/24/i=7/a=075015?key=crossref.2f9ebcbf60c9b51319ea2453102f1ff4

[16] Pai P, Wen B, Naser A and Schulz M 1998 *Journal of Sound and Vibration* **215** 273–296 ISSN 0022460X URL https://linkinghub.elsevier.com/retrieve/pii/S0022460X98916121

[17] Oueini S S and Nayfeh A H 2000 *Journal of Vibration and Control* **6** 999–1016 ISSN 1077-5463 URL http://journals.sagepub.com/doi/10.1177/107754630000600703

[18] Lossouarn B, Deü J F and Kerschen G 2018 *Philosophical Transactions of the Royal Society*

A: Mathematical, Physical and Engineering Sciences **376** 20170142 ISSN 1364-503X URL http://rsta.royalsocietypublishing.org/lookup/doi/10.1098/rsta.2017.0142

[19] Silva T M, Clementino M A, De Marqui C and Erturk A 2018 *Journal of Sound and Vibration* **437** 68–78 ISSN 0022460X URL https://doi.org/10.1016/j.jsv.2018.08.038 https://linkinghub.elsevier.com/retrieve/pii/S0022460X18305455

[20] Lo Feudo S, Touzé C, Boisson J and Cumunel G 2019 *Journal of Sound and Vibration* **438** 33–53 ISSN 0022460X URL https://linkinghub.elsevier.com/retrieve/pii/S0022460X18305868

[21] Fleming A, Behrens S and Moheimani S 2000 *Electronics Letters* **36** 1525 ISSN 00135194 URL https://digital-library.theiet.org/content/journals/10.1049/el_20001083

[22] Habib G and Kerschen G 2016 *Physica D: Nonlinear Phenomena* **332** 1–8 ISSN 01672789 (*Preprint* 1606.01244) URL http://dx.doi.org/10.1016/j.physd.2016.06.001 https://linkinghub.elsevier.com/retrieve/pii/S0167278915300580

[23] Detroux T, Renson L, Masset L and Kerschen G 2015 *Computer Methods in Applied Mechanics and Engineering* **296** 18–38 ISSN 00457825 (*Preprint* 1604.05621) URL http://dx.doi.org/10.1016/j.cma.2015.07.017 https://linkinghub.elsevier.com/retrieve/pii/S0045782515002297

[24] Lossouarn B, Aucejo M, Deü J F and Multon B 2017 *Sensors and Actuators A: Physical* **259** 68–76 ISSN 09244247 URL http://dx.doi.org/10.1016/j.sna.2017.03.030 https://linkinghub.elsevier.com/retrieve/pii/S0924424716309785

[25] Park C H and Inman D J 2003 *Shock and Vibration* **10** 127–133 ISSN 1070-9622 URL http://www.hindawi.com/journals/sv/2003/863252/abs/

[26] Matten G, Collet M, Cogan S and Sadoulet-Reboul E 2014 *Procedia Technology* **15** 84–89 ISSN 22120173 URL http://linkinghub.elsevier.com/retrieve/pii/S2212017314001522 https://linkinghub.elsevier.com/retrieve/pii/S2212017314001522

[27] Horowitz P and Hill W 2015 *The Art of Electronics* 3rd ed (Cambridge University Press) ISBN 978-0-521-37095-0

[28] Apex Microtechnology, Inc 2012 *PA78 Power Operational Amplifier* URL https://www.apexanalog.com/resources/products/pa78u.pdf

[29] Adams D and Allemang R 2000 *Mechanical Systems and Signal Processing* **14** 637–656 ISSN 08883270 URL https://linkinghub.elsevier.com/retrieve/pii/S0888327000912925